

Article

Performance Analysis of LDS Multi Access Technique and New 5G Waveforms for V2X Communication

Imane Khelouani ^{1,2,*}, Fouzia Elbahhar ¹, Raja Ellassali ² and Nouredine Idboufker ²

¹ COSYS-LEOST, University Gustave Eiffel, 59650 Villeneuve d'ascq, France; fouzia.boukour@univ-eiffel.fr

² TIM, ENSA, University of Cadi Ayyad, Marrakech 40000, Morocco; r.ellassali@uca.ma (R.E.); n_idboufker@yahoo.fr (N.I.)

* Correspondence: imane.khelouani@univ-eiffel.fr

Received: 1 May 2020; Accepted: 2 July 2020; Published: 4 July 2020



Abstract: Low Density Signature (LDS) is an emerging non-orthogonal multiple access (NOMA) technique that has never been evaluated under a vehicular channel in order to simulate the environment of a vehicle to everything (V2X) communication. Moreover, the LDS structure has been combined with only Orthogonal Frequency Division Multiplexing (OFDM) and Filter-Bank Multi-Carrier (FBMC) waveforms to improve its performances. In this paper, we propose new schemes where the LDS structure is combined with Universal Filtered Multi-Carrier (UFMC) and Filtered-OFDM waveforms and the Bit Error Rate (BER) is analysed over a frequency selective channel as a reference and over a vehicular channel to analyse the effect of the Doppler shift on the overall performance.

Keywords: V2X; LDS-F-OFDM; LDS-UFMC; EVA channel model

1. Introduction

Vehicular communications have recently caught a lot of attention in the research community thanks to the advantages that they can provide the overall vehicular experience. In fact, several technologies have provided the requirements for this type of communication. Connected to the infrastructure (V2I), to another vehicle (V2V) or to a pedestrian (V2P), the vehicle to everything (V2X), as it is referred to, is a new solution for road users to enhance safety and improve the traffic efficiency. The Long Term Evolution (LTE) as a widely deployed infrastructure is proposed to be extended in order to support the V2X services, namely the LTE-based V2X [1]. The 3rd Generation Partnership Project (3GPP) Release 14 is an evolutionary standard that is dedicated to the LTE-based V2X and published on September 2016 defining two new modes, mode 3 and mode 4 [2,3]. In mode 3, the radio resource is managed by the cellular network, consequently vehicles can only communicate under a cellular coverage. Meanwhile in mode 4, the radio resource is managed autonomously by the vehicle itself for the direct V2V communication overcoming the coverage limitation of mode 3. However, LTE-based V2X standard suffers from severe performance degradation in a high density environment—it does not allow a high number of users access to the network. In addition, LTE-based V2X is based on Single Carrier Frequency Division Multiple Access (SC-FDMA) which requires high complexity equalizers. The ITS-G5 is another standard that is introduced by the European Telecommunications Standards Institute (ETSI) and operates in 5 GHz frequency band [4]. The main advantage of ITS-G5 is its low latency, the short transmission delay is due to the fact that data is being transferred directly between neighbours. However, in best case scenarios, ITS-G5 has a short range of 1 km and is extremely sensitive to dense environment which reduces the total throughput and increases the end-to-end latency. Similar to the IEEE 802.11p US standard, both LTE-based V2X and ITS-G5 rely on Orthogonal Frequency Division Multiplexing (OFDM) on the PHY layer, while maintaining the subcarriers orthogonality

could be challenging in the vehicular environment leading to a high Bit Error Rate (BER). This is why the 5G cellular network can be a promising technology to support the vehicular communications [5], namely New Radio-V2X (NR-V2X).

The 3GPP Release 16 defines the first specifications for NR-V2X sidelink where it supports subcarrier spacings of 15 kHz, 30 kHz, 60 kHz and 120 kHz. Their associations to Cyclic Prefix (CPs) and frequency ranges are as for NR Uplink/Downlink (UL/DL), but using only the CP-OFDM waveform. The modulation schemes available are Quadrature Phase Shift Keying (QPSK), Quadrature Amplitude Modulation 16-(QAM), 64-QAM and 256-QAM [6]. Meanwhile, another study has been published for non-orthogonal multiple access (NOMA) signature candidates [7] proposing some of the main technologies such as Interleaver Division Multiple Access (IDMA) [8–10], Pattern Division Multiple Access (PDMA) [11,12] and Sparse Code Multiple Access (SCMA) [13,14]. However, for V2X communication, no specifications invoke NOMA.

As an efficient multiple access technique, we have chosen to modulate Low Density Signature (LDS) and analyse its performances under a vehicular channel for V2X communication. Its sparse structure enables each user to spread its data over a small subset of subcarriers, which means that a single subcarrier will support only a small number of users or symbols, hence reducing the multiuser interference (MUI). Firstly, it is proposed in [15] for a Code Division Multiple Access (CDMA) system and proves that it can afford a high system overload with affordable complexity. To improve its performances, LDS is enhanced by combining it with OFDM [16] to apply the spreading over OFDM subcarriers and evaluate over a frequency selective channel. Furthermore, the LDS has been recently combined with FBMC [17] and a joint sparse graph receiver combining pulse shaping property, NOMA and channel coding is proposed to improve the overall result at the cost of very high complexity. Although LDS-OFDM and Joint Sparse Graph-Isotropic Orthogonal Transfer Algorithm (JSG-IOTA) have shown improved performance evaluation, these schemes have only been analysed over a frequency selective channel. Our objective is to extend the state-of-art work to evaluate the performance of LDS over a high mobility channel to simulate the vehicular environment for V2X applications and combine it with other advanced 5G waveforms, specifically for an application that requires a high data rate, a medium number of users connected to the network in a certain geographical area and a time of latency smaller than 1 ms [5].

Among these promising 5G waveforms, Universal Filtered Multi-Carrier (UFMC) [18] has drawn attention due to its ability to overcome OFDM shortcomings. By applying properly designed sub-band filtering, UFMC reduces the high out-of-band (OOB) power emission while retaining the simplicity of the conventional OFDM signal. In fact, one of the main advantages of UFMC is its compatibility with the OFDM signals which achieves low system complexity in the NOMA schemes.

Filtered-OFDM [19,20] is also one of the proposed advanced waveforms for the future cellular network. Both UFMC and f-OFDM signals use filtering per subband in order to achieve a low OOB, the main difference is the filter length and its flexibility. F-OFDM uses a long filter with different lengths for each subband (Windowed Sinc filter) exceeding the CP while UFMC signals use short fixed length filters for each subband (Chebyshev filter). In this paper, our goal is to propose a scheme that benefits from the waveforms robustness and multi-carrier transmission combined with the non-orthogonality of a spreading based NOMA to provide a system with less complexity while keeping the transmission model flexible to any future changes and maintaining a certain compatibility with the current techniques. It is why, we have developed a new LDS-UFMC and LDS-F-OFDM schemes in which the LDS spreading is applied to UFMC and f-OFDM signals. Among the different filters that f-OFDM can offer, we adopt computing the Hann, Hamming and Blackman filters thanks to the great performance they shown in terms of BER and OOB reduction [21] and also to provide a better comparison. These schemes will be BER analysed for a V2X communication i.e., a high mobility channel. The multiuser detector will be based on Message Passing Algorithm (MPA) [22]. It will be proved that LDS-F-OFDM outperforms the LDS-OFDM and LDS-UFMC by allowing the filter length to exceed the CP length of OFDM and designing the filter appropriately.

The remainder of this paper is organised as follows. Section 2 introduces the system model of LDS-UFMC. Section 3 is devoted to the LDS-F-OFDM system model. Section 4 presents simulation results of LDS-UFMC and LDS-F-OFDM compared to LDS-OFDM in different environments. Finally, Section 5 concludes this work.

2. LDS-UFMC System Model

In this section, we are going to define the major blocks of an LDS-UFMC system. The LDS-UFMC block diagram is shown in Figure 1. After coding and modulation, the symbols are multiplied with low density spreading sequences then modulated and transmitted simultaneously. Afterwards, spreaded data are shaped into a time-frequency grid. In this configuration, we address the pilots aided channel estimation. For simplicity, we propose to insert the pilots using the Comb Type arrangement. Then, this grid is UFMC modulated using an N-point Inverse Fast Fourier Transform (IFFT) and filtered by a L-length Dolph–Chebyshev filter. At the receiver side, the received signal is UFMC demodulated, then the pilots extraction is performed in order to estimate the channel using the Least Square (LS) method and linear interpolation. The equalizer block uses Zero-Forcing to eliminate the channel effect. The output of the equalizer is passed to the LDS detector where an iterative detection process based on MPA is performed to separate the users' symbols.

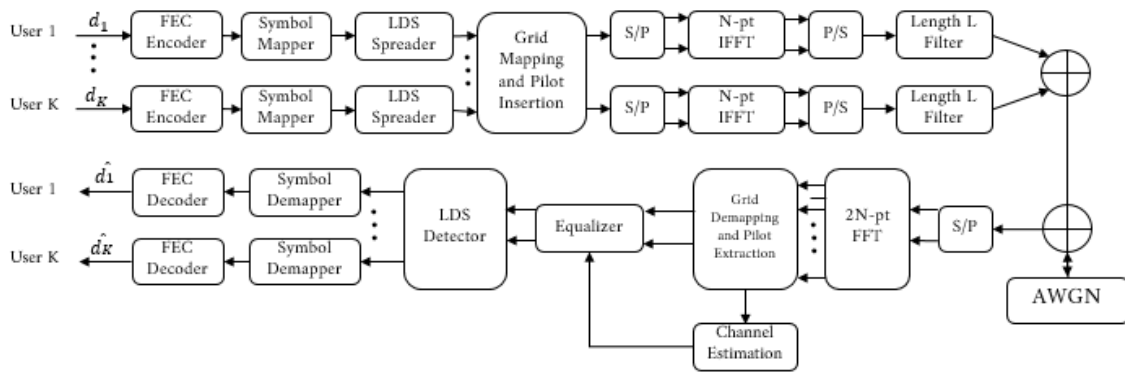


Figure 1. Low Density Signature-Universal Filtered Multi-Carrier (LDS-UFMC) block diagram.

2.1. LDS Spreader

Consider an LDS-UFMC system with K users and the users are indexed as follows; $k = 1, \dots, K$ and all users are assumed to transmit the same number of data streams M and they are indexed as follows; $m = 1, \dots, M$. Assume the number of subcarriers is N , and they are indexed as follows; $n = 1, \dots, N$. We define the spreading matrix of the k th user as:

$$\mathbf{S}_k = [s_{k,1}, \dots, s_{k,M}] \in \mathbb{C}^{N \times M} \tag{1}$$

$s_{k,m} = [s_{k,m}^1, \dots, s_{k,m}^N]^T$ is the sparse vector of length N used to spread the m th symbol of the k th user. Thus, the matrix of spreading of all users can be represented as :

$$\mathbf{S} = [\mathbf{S}_1, \dots, \mathbf{S}_K] \in \mathbb{C}^{N \times MK} \tag{2}$$

Thanks to the sparse nature of this matrix, only a small number of users can share the same subcarrier, we define it as d_c the interference degree. Hence, among N subcarriers only d_v will be used to serve one user, d_v is called the effective spreading gain. Unlike the conventional CDMA system, we require $d_v \ll N$ and $d_c \ll K$. Let \mathbf{a}_k be user's k symbols:

$$\mathbf{a}_k = [a_{k,1}, \dots, a_{k,M}]^T \tag{3}$$

After the spreading process, the signal of the k th user $\mathbf{x}_k = [x_k^1, \dots, x_k^N]^T$ is a vector of length N and can be written as follows:

$$\mathbf{x}_k = \mathbf{S}_k \times \mathbf{a}_k \tag{4}$$

and x_k^n will be the data transmitted over the n th subcarrier by the k th user:

$$x_k^n = \sum_{m=1}^M a_{k,m} s_{k,m}^n \tag{5}$$

Hence, the signal transmitted over the n th subcarrier is given by (6):

$$x^n = \sum_{k \in \xi_n} x_k^n \tag{6}$$

ξ_n is considered as the group of users interfering in the n th subcarrier.

Figure 2 represents the spreading process of the LDS. In this example, we consider that each user transmits one symbol (i.e., $M = 1$). The system transmits over 4 subcarriers and serves 8 users which means that the overloading is at 200%. Each subcarrier is allocated to 4 users ($d_c = 4$), and each user spreads its data over 2 subcarriers ($d_v = 2$). The symbols are the variable nodes and the subcarriers are the functions nodes respectively. The edges that connect the nodes define if a symbol will be spreaded over the adjacent subcarrier. For instance, the first user is connected to subcarriers 1 and 2, consequently, the first symbol will be spreaded over these adjacent subcarriers only. This representation of the spreading process is called the Tanner Graph [16].

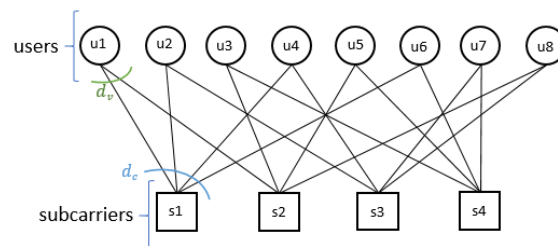


Figure 2. Spreading process of LDS-UFMC system.

2.2. Signal Model

After the LDS spreading, the UFMC modulation is applied to each subcarrier. In fact, UFMC divides the entire bandwidth B of N subcarriers into multiple subbands S_u , each subband consists of Q subcarriers. Hence, the n th subcarrier can now be regarded as the q th subcarrier of the s th subband. After that, the IFFT is performed over the signal of each subband and will be filtered using a L -length prototype filter, usually, the filter is a Dolph–Chebyshev window. The subbands are then superimposed and sent over the channel. The baseband discrete UFMC signal is represented in (7):

$$\mathbf{x}_{LDS-UFMC}[\mathbf{n}] = \sum_{s=0}^{S_u-1} \mathbf{g}_s[\mathbf{n}] \times \mathbf{x}_s[\mathbf{n}] \tag{7}$$

$\mathbf{g}_s[\mathbf{n}]$ defines the filter used in the s th subband :

$$\mathbf{g}_s[\mathbf{n}] = \mathbf{g}[\mathbf{n}] e^{j(2\pi n Q/2)/N} e^{j(2\pi n (S_0 + sQ))/N} \tag{8}$$

where S_0 denotes the starting frequency of the lowest subband and $\mathbf{g}[\mathbf{n}]$ is a well-localised Chebyshev pulse filter of length L . The third term of the equation is the one responsible for frequency shifting

to the appropriate subband. $x_s[n]$ is signal transmitted over the s th group of subcarriers. It can be expressed as follows:

$$x_s[n] = \sum_{q=0}^{Q-1} x^{s,q} e^{j(2\pi nq/2)/N} e^{j(2\pi n(S_0+sQ))/N} \tag{9}$$

Hence, $x^{s,q}$ can be nothing but the signal transmitted over the q th subcarrier of the s th subband and just like in (6), it is given by:

$$x^{s,q} = \sum_{k \in \xi_{s,q}} x_k^{s,q} \tag{10}$$

where $\xi_{s,q}$ is considered as the group of users interfering in the q th subcarrier of the s th subband.

The received signal is represented as follows:

$$y_{LDS-UFMC}[n] = h[n] \times x_{LDS-UFMC}[n] + z[n] \tag{11}$$

where $z[n]$ and $h[n]$ are the additive white gaussian noise with variance σ_z^2 and the channel impulse response respectively. The length of the signal $y_{LDS-UFMC}$ is $N_y = N + L - 1$ due to the convolution with the subband filter, consequently, a $2N$ -point Fast Fourier Transform (FFT) is performed at the UFMC receiver. After the UFMC demodulation process, the input of the LDS Detector corresponding to the n th subcarrier is :

$$Y_n = H_n \sum_{k \in \xi_n} \sum_{m=1}^M a_{k,m} s_{k,m}^n \tag{12}$$

where Y_n and H_n are the $2N$ -point FFT of the time domain signal respectively. In our system, we have chosen to use the equalizer embedded with the LDS detector for a better performance. Regarding the LDS decoding, firstly, the LDS turbo receiver uses MPA and Forward Error Correction (FEC) decoder to find the reliability of the symbols. Secondly, the JSG receiver uses pulse shaping, NOMA and channel coding, however, it is highly complex. For simplicity, we chose to implement the basic LDS detector that uses the Tanner Graph for implementing the MPA receiver in which we consider subcarriers and symbols as function nodes and variable nodes, respectively. Adjacent nodes are connected via edges. Based on an extrinsic manner, each node will update its information containing the reliability of the symbol based on the received reliability from other edges and send it back. After an appropriate number of iterations, the reliability which is the log likelihood ratio (LLR) of the symbols will converge and the symbols are transmitted to the FEC decoder. The major goal behind this complex implementation is to find the value of \hat{a} that maximises the joint a posteriori probability based on the observed signal:

$$\hat{a} = \arg \max_{a \in \mathbb{X}} p(a|y) \tag{13}$$

where \mathbb{X} is the modulation constellation. The first LLR update can be written as follows:

$$\begin{aligned} \ell_{c_n \leftarrow u_k}(a_k) &= \log \frac{P_{\text{ext},n}(a_k = +1)}{P_{\text{ext},n}(a_k = -1)} \\ &= \sum_{m \in \varphi_k \setminus n} \ell_{c_m \rightarrow u_k} \end{aligned}$$

where u nodes are the variable nodes and c nodes are the function nodes, hence $\ell_{c_n \leftarrow u_k}$ is the message sent from u_k node to the c_n node and $\ell_{c_n \rightarrow u_k}$ message sent from c_n node to the u_k node, respectively. It is clear from the above equation that the update of $\ell_{c_n \leftarrow u_k}(a_k)$ is dependent to all nodes besides the node n i.e., $m \in \varphi_k \setminus n$, hence, the notation of extrinsic update. Second Update can be calculated as follow:

$$\ell_{c_n \rightarrow u_k}(a_k) = \log \left(\sum_{a_n \in X} P(y_n | a_n) \prod_{l \in \xi_n \setminus k} P_n(a_l) \right)$$

where φ_k is the group of subcarriers allocated to the k th user and $P(y_n|a_n)$ is the channel observation function at subcarrier y_n . Further explanations are provided in [22].

3. LDS-F-OFDM System Model

Based on the same LDS spreader used in LDS-UFMC, LDS-F-OFDM applies Filtered-OFDM waveform on the users' spreaded signals and transmits them over the channel. The LDS based on f-OFDM block diagram is presented in Figure 3. As depicted, the signal is mapped into a time-frequency grid and then the pilots are inserted for channel estimation. Afterwards, a N-point IFFT is performed to transfer the grid from the frequency domain to the time domain, data is then serialised and CP is added to combat Inter Symbol Interference (ISI) effect. Like UFMC, the main advantage of f-OFDM is its compatibility with OFDM, with a difference of passing the signal through a long length filter before the transmission. Extended over the CP, the filter helps to lower the high OOB radiation while maintaining the OFDM orthogonality between the subcarriers. Usually, a truncated sinc window is used as a shaping filter, however in our system we have chosen to implement other types of filters for a better comparison. For LDS-F-OFDM, we consider all the subcarriers as one subband to lower the overall complexity. Therefore, our transmitted signal is an OFDM modulated signal passed through an appropriate shaped filter. Without loss of generality, the signal expression can be written as follows:

$$x_{LDS-F-OFDM}[n] = x_{LDS-OFDM}[n] \times f_{TX}[n] \tag{14}$$

where $f_{TX}(n)$ represents the well-designed filter and $x_{LDS-OFDM}[n]$ is the discrete LDS-OFDM signal after the spreading and modulation, it is represented as follows:

$$x_{LDS-OFDM}[n] = \sum_{q=0}^{N-1} x^q e^{j2\pi nq/N} \tag{15}$$

The transmitted signal is given by (16):

$$x_{LDS-F-OFDM}[n] = \sum_{q=0}^{N-1} x^q e^{j2\pi nq/N} \times f_{TX}[n] \tag{16}$$

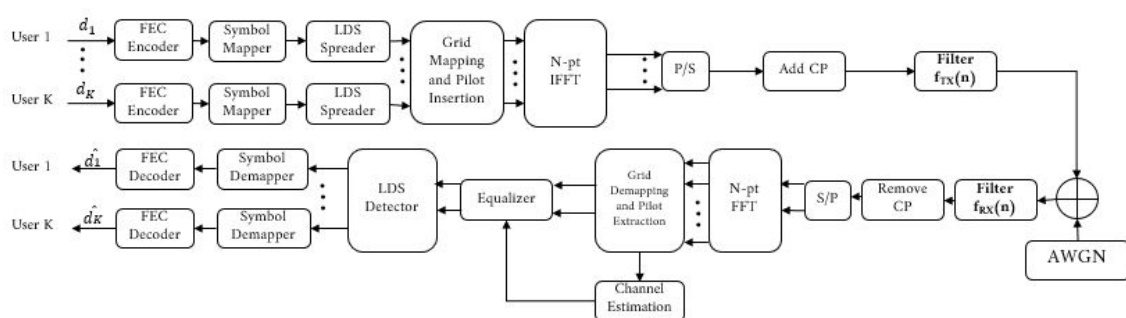


Figure 3. LDS-F-OFDM block diagram.

3.1. Filter Design

The main reason behind the filtering is to eliminate the side lobes for an efficient transmission, it is why filters based on cardinal sin are taken into consideration thanks to their sharp filter response. However, the filter characteristic should be truncated due to its infinite impulse response. As a result, we obtain a finite sinc filter and a window pulse $w[n]$ is applied to smooth its transitions. Once the filter is computed, it should be shifted around the central frequency of the subband.

$$p[n] = \text{sinc}\left(\frac{W + 2\delta_W n}{N}\right) \tag{17}$$

$$p_B[n] = \frac{p[n]w[n]}{\sum_n |p[n]w[n]|} \quad (18)$$

$$f_{TX}[n] = p_B[n]e^{\frac{j2\pi n f_c}{N\Delta_f}} \quad (19)$$

where W is the number of active subcarriers, δ_W is the tone offset, N is the FFT size, f_c is the frequency of the centre subcarrier in the baseband and Δ_f is the subcarrier spacing. The window function of the chosen windows are defined in Table 1.

Table 1. Window function of the filters.

Window	Window Function
Hann	$w[n] = 0.5 \times (1 + \cos(\frac{2\pi n}{L-1}))$
Hamming	$w[n] = \frac{25}{46} + \frac{21}{45} \times \cos(\frac{2\pi n}{L-1})$
Blackman	$w[n] = \frac{7938}{18608} + \frac{9240}{18608} \times \cos(\frac{2\pi n}{L-1}) + \frac{1430}{18608} \times \cos(\frac{4\pi n}{L-1})$

At the receiver side, a matching filter $f_{RX}[n]$ to the transmission filter $f_{TX}[n]$ is performed at the received signal, after that the CP is removed and the signal is transmitted to an OFDM receiver. After the grid demapping and pilot extraction, channel estimation is performed based on the pilots. The output data are then considered as the input of LDS detector explained in Section 2.

4. Performance Evaluation

In this section, we propose to compare the performances of the proposed LDS-F-OFDM and LDS-UFMC schemes with the LDS-OFDM over a vehicular channel with different speed limits and over a multipath fading channel. The main simulation parameters are used to match the 3GPP Release 16 standard. Based on 3GPP Release 16, we have fixed the total bandwidth to $B = 10$ MHz and a carrier frequency of $f_c = 5.9$ GHz to match the NR-V2X operating bands in FR1 [23]. Table 2 summarises the simulation parameters.

Table 2. Simulation parameters.

Parameters	Symbol	Value
Release 16 Parameters		
Bandwidth	B	10 MHz
Carrier frequency	f_c	5.9 GHz
Number of symbols	N_{sym}	14
Subcarriers spacing	Δ_f	15 kHz 30 kHz
Number of Resource Blocks	N_{RB}	52
		24
FFT Size	N_{FFT}	1024
		512
Cyclic Prefix Length	L_{CP}	72
		36

Table 2. Cont.

Parameters	Symbol	Value
Pilots Parameters		
Pilots Arrangement	-	Comb type
Pilots Spacing	N_{ps}	4
Number of Pilots per symbol	N_p	156 72
UFMC		
Filter Length	L_U	65 33
Filter Type	-	Dolph-Chebyshev
Side Lobe Attenuation	-	50 dB
Number of Subbands	S	52 24
Subband size	Q	12
F-OFDM		
Filter Length	L_F	513 257
Window function	-	Hann Hamming Blackman
LDS Scheme Parameters		
Effective Processing gain	d_v	3
Interference Pattern	d_c	3
Number of Users	N_u	468 216
Modulation	-	BPSK

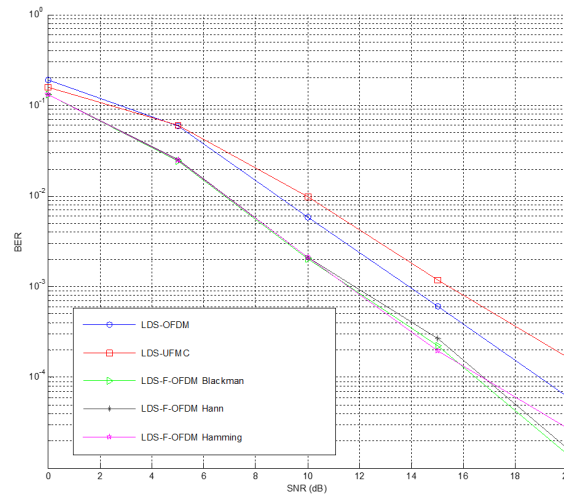
No error correction is employed, so the evaluation is carried out for uncoded bits. The LDS spreading matrix is generated randomly for all the simulated schemes. However, we do believe that a well designed matrix with small number of cycle-of-four and a high girth can achieve better performance.

In order to respect the 3GPP recommendations, no overloading scenario is deployed due to the use of pilots and the waveforms offset. We have overcome this circumstance by respecting the rule of interfering several users in the same resource and allocating a few subcarriers to the same user i.e., respecting the LDS structure to justify these new schemes performances. The maximum number of iterations of the LDS detector is ten.

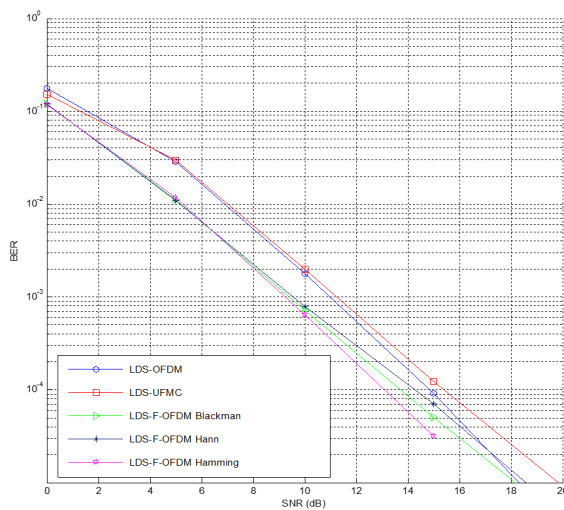
The first channel we have chosen to evaluate the performance of these schemes is the Tapped Delay Line model, specifically the TDL-A channel. The TDL-A channel model has a Doppler spectrum which is characterised by a Jake's spectrum shape. The Power Delay Profile (PDP) of the model is presented in [24] and the delay spread used to scale the normalised taps delays is $D_s = 93$ ns. This delay spread is chosen to correspond to a short delay profile in an Urban Macro environment for a 5.9 GHz carrier frequency.

Figure 4 depicts the simulation results of LDS-F-OFDM and LDS-UFMC over TDL-A channel. We first fix the bandwidth at $B = 10$ MHz, then we investigate the schemes under two systems, the first with 1024 subcarriers and $\Delta_f = 15$ kHz subcarrier spacing and the second with 512 subcarriers and $\Delta_f = 30$ kHz. According to the simulation results, the LDS-F-OFDM shows better performance over both LDS-UFMC and LDS-OFDM. The fact that the f-OFDM subband regroups all the available

subcarriers concentrates the energy in one main lobe. This results in less ISI, and thanks to the LDS structure, the MUI are eliminated, thus, reducing the overall interference. Hence, it is expected that the f-OFDM with the LDS structure achieve a better BER performance. Meanwhile, LDS-UFMC shows a slight performance degradation compared to LDS-OFDM. However, UFMC offers lower OOB and the main advantage of UFMC is the increased spectral efficiency. Consequently, a trade-off must be taken in consideration depending on the requirements of the application.



(a) $\Delta_f = 15$ kHz



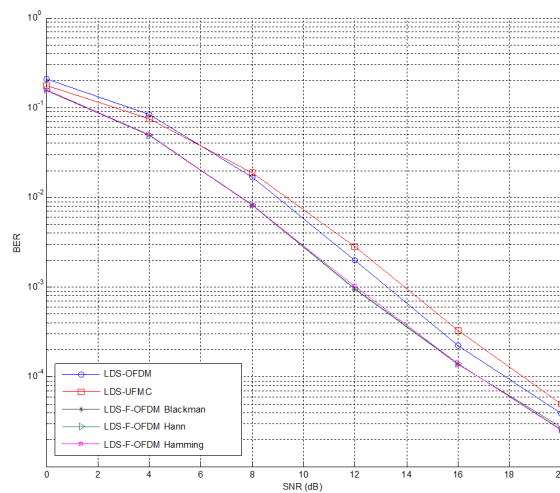
(b) $\Delta_f = 30$ kHz

Figure 4. Performance of the proposed schemes over a Tapped Delay Line (TDL)-A channel.

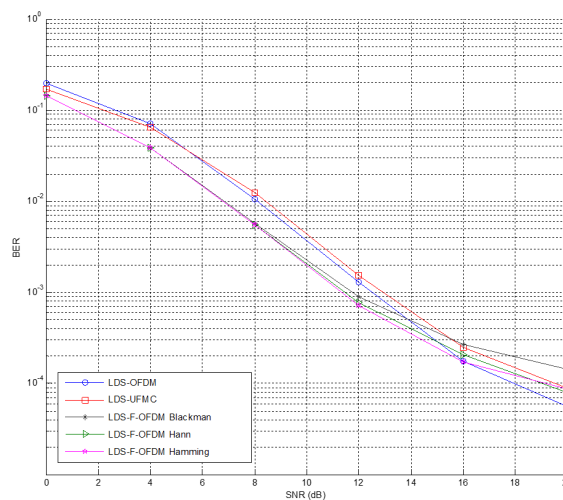
The second and main channel used to simulate these schemes is the Extended Vehicular A (EVA) model channel, its power delay profile is provided in [25]. Similarly to the TDL-A model, the EVA model is characterised by a Jake’s Doppler spectrum and the maximum speed simulated is 300 km/h, hence the maximum Doppler shift $f_d = 556$ Hz and specifically modelled to simulate a vehicular channel.

Figure 5a shows the BER performance of the LDS-F-OFDM and LDS-UFMC compared to LDS-OFDM over an EVA channel with a computed speed of 100 km/h which means that the maximum Doppler shift is $f_d = 185$ Hz with a subcarrier spacing of $\Delta_f = 15$ kHz and an FFT size of 1024, hence only 468 subcarriers left for data transmissions. For simplicity, we consider 468 users each sending one BPSK modulated symbol with a power of 1 Watt. In fact, this is the worst loading scenario where we have the number of users equal to the number of subcarriers allocated to data transmission which

means that each user will be able to send only one symbol. It can be noticed that the LDS-F-OFDM slightly outperforms once more both LDS-OFDM and LDS-UFMC with its all different types of filters deployed. While Hann, Hamming and Blackman windows achieve almost the same BER performance, Hann window function is the filter susceptible to give better OOB performance. In terms of spectral efficiency, LDS-UFMC compared to LDS-F-OFDM and LDS-OFDM comes first due to the removal of the CP. However, observing the used subcarriers for data transmission due to the use of the pilot with only 4 subcarrier spacing, we notice the overall degraded spectral efficiency. This is completely justified by the need of an efficient channel estimation because of the high changing nature of the channel.



(a) $\Delta_f = 15$ kHz



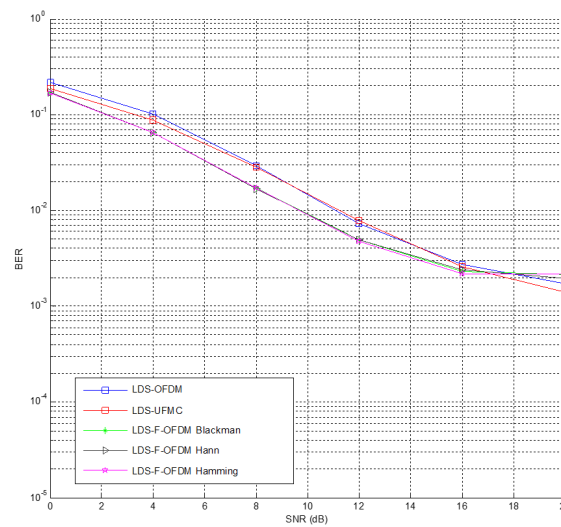
(b) $\Delta_f = 30$ kHz

Figure 5. Performance of the proposed schemes over an Extended Vehicular A (EVA) channel with speed of 100 km/h.

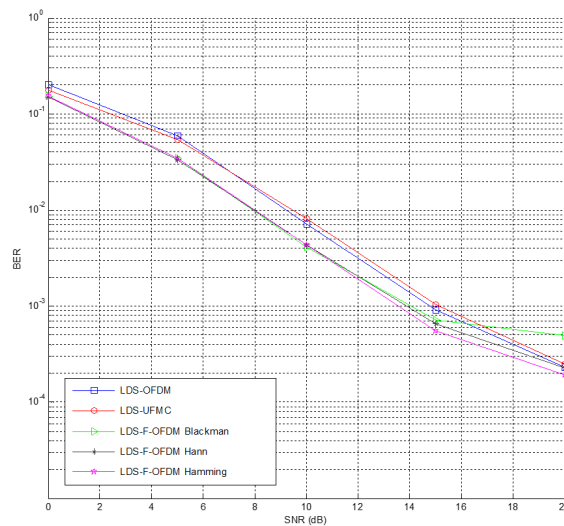
The BER performance of the proposed schemes with a computed speed of 100 km/h and a subcarrier spacing of $\Delta_f = 30$ kHz and 512 subcarriers is presented in Figure 5b. It is worth noting that LDS-F-OFDM shows again better performance at low SNR, while at higher SNR, all the proposed schemes face slight performance degradation. In fact, while employing higher subcarrier spacing to combat the Doppler shift, the spectral efficiency is reduced and also the number of subcarriers allocated to pilots is reduced (156 subcarriers in the first system vs. 72 in the second). Consequently, the channel estimation will not be as efficient as in the first system. Furthermore, in order to investigate

how the LDS-F-OFDM and LDS-UFMC can be affected by the mobility, the schemes are also simulated over an EVA channel with a speed of 300 km/h.

Figure 6a,b represents the simulation results for $\Delta_f = 15$ kHz and $\Delta_f = 30$ kHz, respectively. It can be seen that LDS-F-OFDM shows better performances than LDS-OFDM and LDS-UFMC in low SNR. Moreover, all the techniques demonstrate huge improvements in the second system with $\Delta_f = 30$ kHz subcarrier spacing than the first. Thanks to the large subcarrier spacing, the Doppler shift does not impact severely the subcarriers orthogonality. In addition, comparing Figure 5a with Figure 6a, all the techniques face severe performance degradation due to the high mobility of the UEs. Meanwhile, Figure 5b with Figure 6b presents almost the same BER performances thanks to the large subcarrier spacing.



(a) $\Delta_f = 15$ kHz

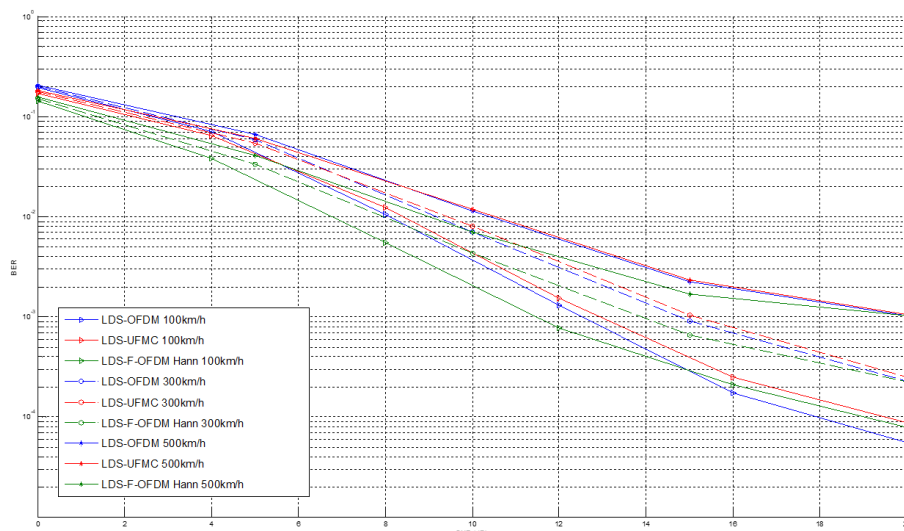


(b) $\Delta_f = 30$ kHz

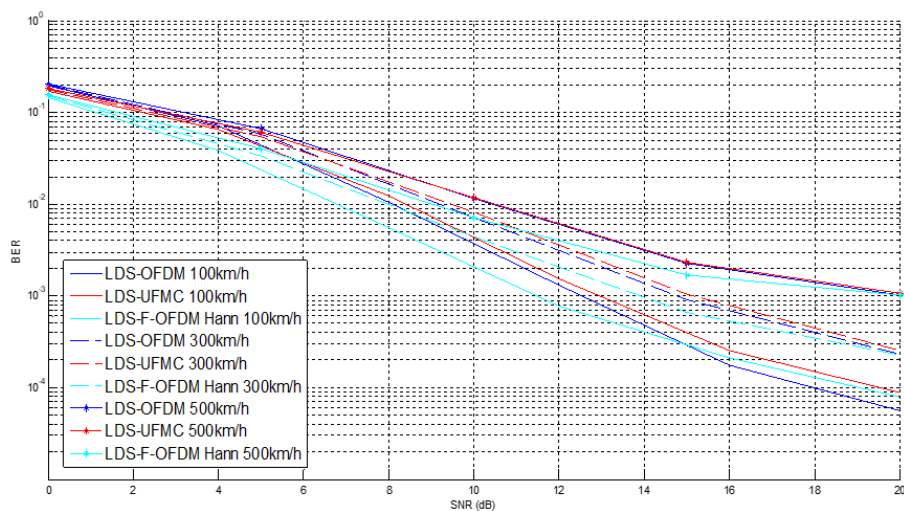
Figure 6. Performance of the proposed schemes over an EVA channel with speed of 300 km/h.

Figure 7 depicts the comparison of the proposed schemes over the EVA channel with different speed limits with both systems. We have chosen to evaluate the schemes also over the EVA channel with a 500 km/h velocity and analyse the degradation of the performance in such an environment. Obviously, the performance decreases due to the high speed, however as shown in Figure 7b i.e., with a large subcarrier spacing, both LDS-F-OFDM and LDS-UFMC seem to suffers less. Meanwhile

with $\Delta_f = 15$ kHz, all the techniques seem unable to converge at high speed. To improve this, other receivers can be considered such as the JSG and Expectation Propagation Algorithm EPA receivers.



(a) $\Delta_f = 15$ kHz



(b) $\Delta_f = 30$ kHz

Figure 7. Schemes comparison over the EVA channel with different speed limits.

5. Conclusions

In this paper, we have proposed two efficient multiple access techniques namely LDS-F-OFDM and LDS-UFMC in which the LDS structure is combined with the new 5G waveforms. First of all, we have presented the state-of-art of the previous work done on LDS and we have detailed the transmitters and receivers of these new schemes. Then, we have highlighted our contribution that consists in evaluating these new schemes over different types of channels, specifically, a vehicular channel with a high mobility. Simulation results show that LDS-F-OFDM significantly achieves higher performance improvements compared to LDS-OFDM and LDS-UFMC in all scenarios, while maintaining an affordable complexity at the transmitter and the receiver side. The improvements are directly related to the advantages that f-OFDM waveform offers by addressing the adequate filter. In future work, we propose to analyse these schemes with different types of receivers in manner to reduce the complexity and to improve the performances. Some of the receivers that can be found in the literature are the SIC-MPA where we combine SIC and MPA to reduce the overall complexity and the JSG receiver which is a very high complex receiver but provides a lot of improvements to the

system. Furthermore, we consider evaluating these schemes over different vehicular channels such as a confined channel and with different channel specifications considering the other operating band of FR1 i.e., 25 GHz.

Author Contributions: Conceptualisation, I.K., R.E., F.E. and N.I.; methodology, I.K., R.E. and F.E.; software, I.K.; validation, R.E., F.E. and N.I.; formal analysis, R.E. and F.E.; investigation, I.K., R.E. and F.E.; resources, R.E. and F.E.; writing—original draft preparation, I.K.; writing—review and editing, I.K.; supervision, R.E., F.E. and N.I.; project administration, R.E. and F.E.; funding acquisition, R.E. and F.E. All authors have read and agreed to the published version of the manuscript.

Funding: The present research work has been supported by the European project SECREDAS funded ECSEL. The preliminary results were partly supported by ELSAT project. ELSAT 2020 project is co-financed by the European Union with the European Regional Development Fund, the French state and the Hauts de France Region Council.

Conflicts of Interest: The authors declare no conflict of interest.

Abbreviations

The following abbreviations are used in this manuscript:

OFDM	Orthogonal Frequency Division Multiplexing
FBMC	Filter-Bank Multi-Carrier
UFMC	Universal Filtered Multi-Carrier
BER	Bit Error Rate
LTE	Long Term Evolution
3GPP	3rd Generation Partnership Project
SC-FDMA	Single Carrier Frequency Division Multiple Access
ETSI	European Telecommunications Standards Institute
NR-V2X	New-Radio V2X
CP	Cyclic Prefix
UL	Uplink
DL	Downlink
QPSK	Quadrature Phase Shift Keying
QAM	Quadrature Amplitude Modulation
IDMA	Interleaver Division Multiple Access
PDMA	Pattern Division Multiple Access
SCMA	Sparse Code Multiple Access
CDMA	Code Division Multiple Access
JSG-IOTA	Joint Sparse Graph-Isotropic Orthogonal Transfer Algorithm
MPA	Message Passing Algorithm
FEC	Forward Error Correction
EPA	Expectation Propagation Algorithm
IFFT	Inverse Fast Fourier Transform
LS	Least Square
FFT	Fast Fourier Transform
ISI	Inter Symbol Interference
OOB	Out Of Band
PDP	Power Delay Profile
EVA	Extended Vehicular A

References

1. Sun, S.; Hu, J.; Peng, Y.; Pan, X.; Zhao, L.; Fang, J. Support for vehicle-to-everything services based on LTE. *IEEE Wirel. Commun.* **2016**, *23*, 4–8. [[CrossRef](#)]
2. Molina-Masegosa, R.; Gozalvez, J. LTE-V for Sidelink 5G V2X Vehicular Communications: A New 5G Technology for Short-Range Vehicle-to-Everything Communications. *IEEE Veh. Technol. Mag.* **2017**, *12*, 30–39. [[CrossRef](#)]

3. Gonzalez-Martín, M.; Sepulcre, M.; Molina-Masegosa, R.; Gozalvez, J. Analytical Models of the Performance of C-V2X Mode 4 Vehicular Communications. *IEEE Trans. Veh. Technol.* **2019**, *68*, 1155–1166. [[CrossRef](#)]
4. Festag, A. Standards for vehicular communication—From IEEE 802.11p to 5G. *Elektrotech. Inftech.* **2015**, *132*, 409–416. [[CrossRef](#)]
5. Anwar, W.; Franchi, N.; Fettweis, G. Physical Layer Evaluation of V2X Communications Technologies: 5G NR-V2X, LTE-V2X, IEEE 802.11bd, and IEEE 802.11p. In Proceedings of the 2019 IEEE 90th Vehicular Technology Conference (VTC2019-Fall), Honolulu, HI, USA, 22–25 September 2019; pp. 1–7.
6. 3GPP TR 37.985. Overall Description of Radio Access Network (RAN) Aspects for Vehicle-to-Everything (V2X) Based on LTE and NR. 3rd Generation Partnership Project; Technical Specification Group Radio Access Network. Available online: <https://www.3gpp.org> (accessed on 2 April 2020).
7. 3GPP TR 38.812. Study on Non-Orthogonal Multiple Access (NOMA) for NR. 3rd Generation Partnership Project; Technical Specification Group Radio Access Network. Available online: <https://www.3gpp.org> (accessed on 2 April 2020).
8. Ping, L.; Liu, L.; Wu, K.; Leung, W.K. Interleave division multiple-access. *IEEE Trans. Wirel. Commun.* **2006**, *5*, 938–947. [[CrossRef](#)]
9. Chen, Y.; Schaich, F.; Wild, T. Multiple Access and Waveforms for 5G: IDMA and Universal Filtered Multi-Carrier. In Proceedings of the 2014 IEEE 79th Vehicular Technology Conference (VTC Spring), Seoul, Korea, 18–21 May 2014; pp. 1–5.
10. Li, B.; Du, R.; Kang, W.; Liu, G. Multi-User Detection for Sporadic IDMA Transmission Based on Compressed Sensing. *Entropy* **2017**, *19*, 334.
11. Zeng, J.; Li, B.; Su, X.; Rong, L.; Xing, R. Pattern division multiple access (PDMA) for cellular future radio access. In Proceedings of the 2015 International Conference on Wireless Communications & Signal Processing (WCSP), Nanjing, China, 15–17 October 2015; pp. 1–5.
12. Ren, B.; Wang, Y.; Dai, X.; Niu, K.; Tang, W. Pattern matrix design of PDMA for 5G UL applications. *China Commun.* **2016**, *13*, 159–173. [[CrossRef](#)]
13. Nikopour, H.; Yi, E.; Bayesteh, A.; Au, K.; Hawryluck, M.; Baligh, H.; Ma, J. SCMA for downlink multiple access of 5G wireless networks. In Proceedings of the 2014 IEEE Global Communications Conference, Austin, TX, USA, 8–12 December 2014; pp. 3940–3945.
14. Liu, B.; Zhang, L.; Xin, X. Non-orthogonal optical multicarrier access based on filter bank and SCMA. *Opt. Express* **2015**, *23*, 27335–27342. [[CrossRef](#)] [[PubMed](#)]
15. Hoshyar, R.; Wathan, F.P.; Tafazolli, R. CTH06-4: Novel Low-Density Signature Structure for Synchronous DS-CDMA Systems. In Proceedings of the IEEE Globecom 2006, San Francisco, CA, USA, 28–30 November 2006; pp. 1–5.
16. Hoshyar, R.; Razavi, R.; Al-Imari, M. LDS-OFDM an Efficient Multiple Access Technique. In Proceedings of the 2010 IEEE 71st Vehicular Technology Conference, Taipei, Taiwan, 16–19 May 2010; pp. 1–5.
17. Wen, L.; Xiao, P.; Razavi, R.; Imran, M.A.; Al-Imari, M.; Maaref, A.; Lei, J. Joint Sparse Graph for FBMC/OQAM Systems. *IEEE Trans. Veh. Technol.* **2018**, *67*, 6098–6112. [[CrossRef](#)]
18. Vakilian, V.; Wild, T.; Schaich, F.; Brink, S.T.; Frigon, J.F. Universal filtered multi-carrier technique for wireless systems beyond LTE. In Proceedings of the IEEE Globecom Workshops (GC Wkshps), Atlanta, TX, USA, 9–13 December 2013.
19. Abdoli, J.; Jia, M.; Ma, J. Filtered OFDM: A new waveform for future wireless systems. In Proceedings of the 2015 IEEE 16th International Workshop on Signal Processing Advances in Wireless Communications (SPAWC), Stockholm, Sweden, 28 June–1 July 2015; pp. 66–70.
20. Zhang, L.; Ijaz, A.; Xiao, P.; Molu, M.M.; Tafazolli, R. Filtered OFDM Systems, Algorithms, and Performance Analysis for 5G and Beyond. *IEEE Trans. Commun.* **2018**, *66*, 1205–1218. [[CrossRef](#)]
21. Thakre, A. Optimal Filter Choice for Filtered OFDM. In Proceedings of the 2019 3rd International Conference on Electronics, Communication and Aerospace Technology (ICECA), Coimbatore, India, 12–14 June 2019; pp. 1035–1039. [[CrossRef](#)]
22. Hoshyar, R.; Wathan, F.P.; Tafazolli, R. Novel Low-Density Signature for Synchronous CDMA Systems Over AWGN Channel. *IEEE Trans. Signal Process.* **2008**, *56*, 1616–1626. [[CrossRef](#)]
23. 3GPP TR 38.886. V2X Services Based on NR; User Equipment (UE) Radio Transmission and Reception. 3rd Generation Partnership Project; Technical Specification Group Radio Access Network. Available online: <https://www.3gpp.org> (accessed on 2 April 2020). [[CrossRef](#)]

24. 3GPP TR 38.900. Study on Channel Model for Frequency Spectrum above 6 GHz. 3rd Generation Partnership Project; Technical Specification Group Radio Access Network. Available online: <https://www.3gpp.org> (accessed on 2 April 2020).
25. 3GPP TS 36.101. Evolved Universal Terrestrial Radio Access (E-UTRA); User Equipment (UE) Radio Transmission and Reception. 3rd Generation Partnership Project; Technical Specification Group Radio Access Network. Available online: <https://www.3gpp.org> (accessed on 2 April 2020).



© 2020 by the authors. Licensee MDPI, Basel, Switzerland. This article is an open access article distributed under the terms and conditions of the Creative Commons Attribution (CC BY) license (<http://creativecommons.org/licenses/by/4.0/>).